European Journal of Medicinal Chemistry 90 (2015) 809–821

Contents lists available at ScienceDirect

European Journal of Medicinal Chemistry

journal homepage: http://www.elsevier.com/locate/ejmech

Original article

Multimodal biopanning of T7 phage-displayed peptides reveals angiomotin as a potential receptor of the anti-angiogenic macrolide Roxithromycin

Kaori Takakusagi [a, 1, 2], Yoichi Takakusagi [a, *, 1, 3], Takahiro Suzuki [b, 4], Aya Toizaki [b], Aiko Suzuki [a], Yaichi Kawakatsu [a], Madoka Watanabe [a], Yukihiro Saito [c], Ryushi Fukuda [c], Atsuo Nakazaki [b, 5], Susumu Kobayashi [b], Kengo Sakaguchi [a], Fumio Sugawara [a, *]

[a] Department of Applied Biological Science, Faculty of Science and Technology, Tokyo University of Science, 2641 Yamazaki, Noda, Chiba 278-8510, Japan
[b] Faculty of Pharmaceutical Sciences, Tokyo University of Science, 2641 Yamazaki, Noda, Chiba 278-8510, Japan
[c] Meiwafosis Co. Ltd., 1-14-2 Shinjuku, Tokyo 160-0022, Japan

ARTICLE INFO

Article history:
Received 17 September 2014
Received in revised form
6 December 2014
Accepted 9 December 2014
Available online 12 December 2014

Keywords:
Roxithromycin
T7 phage display
QCM-D
RELIC
Angiogenesis
Angiomotin

ABSTRACT

Roxithromycin (RXM) is a semi-synthetic fourteen-membered macrolide antibiotic that shows anti-angiogenic activity in solid tumors. In the present study, we conducted biopanning of T7 phage-displayed peptides either on a 96-well formatted microplate, a flow injection-type quartz-crystal microbalance (QCM) biosensor, or a cuvette-type QCM. RXM-selected peptides of different sequence, length and number were obtained from each mode of screening. Subsequent bioinformatics analysis of the RXM-selected peptides consistently gave positive scores for the extracellular domain (E458–T596) of angiomotin (Amot), indicating that this may comprise a binding region for RXM. Bead pull down assay and QCM analysis confirmed that RXM directly interacts with Amot *via* the screen-guided region, which also corresponds to the binding site for the endogenous anti-angiogenic inhibitor angiostatin (Anst). Thus, multimodal biopanning of T7PD revealed that RXM binds to the extracellular domain on Amot as a common binding site with Anst, leading to inhibition of angiogenesis-dependent tumor growth and metastasis. These data might explain the molecular basis underlying the mechanism of action for the anti-angiogenic activity of RXM.

1. Introduction

Roxithromycin (RXM) (Fig. 1) is a macrolide antibiotic in clinical use, which inhibits polypeptide biosynthesis in bacteria [1,2]. This compound consists of a fourteen-membered macrocyclic core bound to two sugar moieties at positions 3 and 5. The methoxy-ethoxy-methyloxime group at position 9 is a distinctive feature of RXM among the macrolide antibiotics [1]. In addition to its antibacterial effects, RXM has been reported to possess various biological activities, such as anti-inflammatory or anti-tumor effects [3], which suggest the existence of molecular target(s) among host human proteins. In particular, the anti-angiogenic effect of RXM has been investigated in detail [3–8]. RXM inhibits vascular endothelial cell proliferation, migration and differentiation into capillary-like structures *in vitro* [4,6–8]. Furthermore, RXM delays the growth of solid tumors by inhibiting angiogenesis, and has been shown to prevent cancer metastases *in vivo* [6,7,9]. Moreover, expression of vascular endothelial growth factor (VEGF), interleukin (IL) production and neutrophil recruitment are all suppressed by RXM treatment [4,5,10,11].

* Corresponding authors.
E-mail addresses: tkksg@rs.noda.tus.ac.jp (Y. Takakusagi), sugawara@rs.noda.tus.ac.jp (F. Sugawara).
[1] These authors contributed equally to this article.
[2] Center for Biologics Evaluation and Research (CBER), Food and Drug Administration (FDA), Rockville, MD, USA.
[3] National Cancer Institute (NCI), National Institutes of Health (NIH), Bethesda, MD, USA.
[4] Department of Chemistry, Faculty of Science, Hokkaido University, Hokkaido, Japan.
[5] Graduate School of Bioagricultural Sciences, Nagoya University, Aichi, Japan.

http://dx.doi.org/10.1016/j.ejmech.2014.12.015
0223-5234/

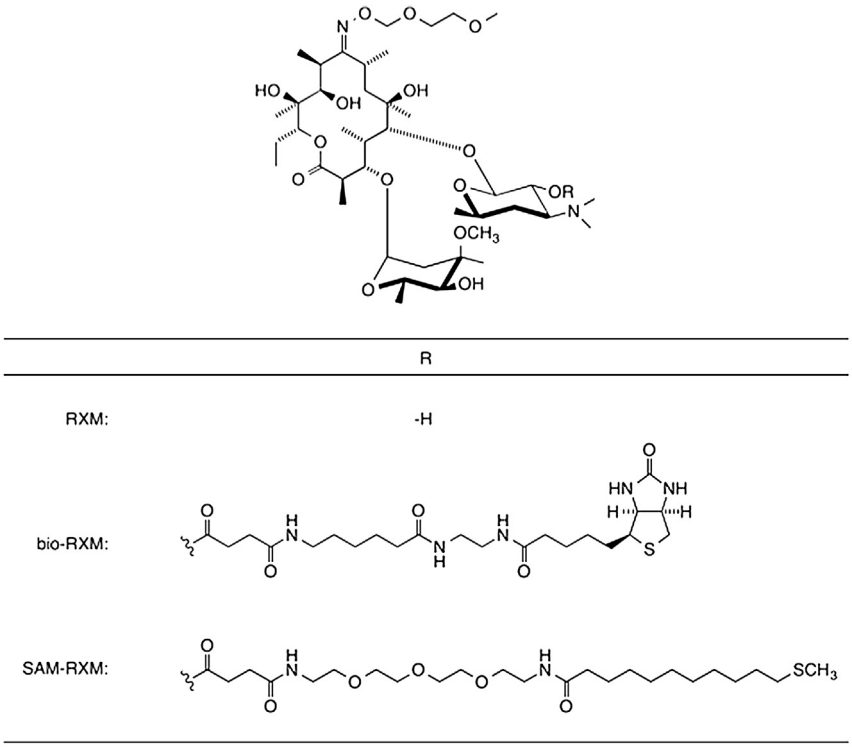

Fig. 1. Structure of RXM and its derivatives used in this study. The bio-RXM was applied to a streptavidin-coated 96-well microplate and avidin agarose beads for RXM immobilization. The SAM-RXM was used for RXM immobilization on the gold electrode surface of a QCM or QCM-D sensor chip.

Identification of RXM binding protein will greatly assist in determining the mode of action of RXM as well as elucidating the molecular basis of adsorption, distribution, metabolism, excretion and toxicity (ADMET) *in vivo*. Here, we employed the T7 phage display (T7PD) system to reveal the direct binding proteins of RXM. In this strategy, drug-recognizing peptides or proteins are affinity-selected from a T7 phage-displayed library by repeated rounds of selection called biopanning. By sequencing part of the recovered T7 phage DNA (gene10) that encodes the T7 capsid protein, the corresponding drug-recognizing amino acid sequence displayed on the capsid can be clearly determined [12]. The obtained amino acid sequence is then analyzed using an appropriate algorithm, such as FASTA or RELIC search engines [13,14] to identify the corresponding drug-recognizing protein species as well as likely region of the molecule that interacts with the drug [12,15–20]. Unlike other proteomics approaches, T7PD facilitates a comprehensive screen for binding proteins of up to 1200 amino acids in length together with identification of the likely binding site(s). Importantly, the technique is applicable even if the target protein is membrane-associated or disordered [12]. Furthermore, PD technology can identify relatively weak binding interactions, as observed for many macrolide compounds that exhibit diverse bioactivities [21,22]. The design of the screening protocol, such as the type of platform employed, drug immobilization chemistry used, type of phage library screened and panning conditions, may dramatically improve the throughput and accuracy of biopanning [12].

In this study, T7PD biopanning using three different modalities were employed to identify direct binding targets of RXM. Firstly, we utilized a classical method using a streptavidin-coated polystyrene microplate with repeated rounds of selection of a T7 phage-displayed protein library constructed from cDNA [23]. Secondly, selection of T7 phage-displayed random peptides on a quartz-crystal microbalance using a flow injection-type dissipation monitoring system (QCM-D) was employed [24,25]. Thirdly, we used a cuvette-type QCM biosensor-based one-cycle biopanning procedure of drug-recognizing short peptides as reported previously [15,20,26]. Affinity selection using all three modalities identified an extracellular domain on angiomotin (Amot), a vascular endothelial cell receptor, as a potential direct binding site of RXM. Amot is a receptor of an endogenous anti-angiogenic factor angiostatin (Anst), which exerts a strong effect in inducing the migration and tubule formation from endothelial cells as well as promoting angiogenesis [27–31]. In addition, like RXM, Anst targets neutrophils that express Amot and inhibits their activation and migration [11,32,33]. Indeed, avidin-bead pull down assay and QCM analysis confirmed the direct binding of RXM to Amot through the screen-guided extracellular domain (BIG3), highlighting that RXM binds to the common extracellular domain with Anst. These data might explain the molecular basis underlying the mode of action for the anti-angiogenic effect of RXM, which may provide guidance for further experimentation and clinical investigation of tumor chemotherapy by RXM.

2. Results

2.1. Chemistry

2.1.1. Design and synthesis of RXM derivatives

In order to immobilize RXM onto a streptavidin-coated microplate or avidin-conjugated agarose beads, a biotinylated derivative of RXM (Fig. 1) was prepared according to our previous report [21]. An RXM derivative that forms a self-assembled monolayer (SAM) on gold surfaces (Fig. 1, Scheme 1) was also synthesized to enable immobilization of RXM on the gold electrode of the QCM sensor chip [15,20,26,34]. In these cases, C11 alkyl chains connected with a disulfide bond were used as a scaffold for SAM. To avoid intricate

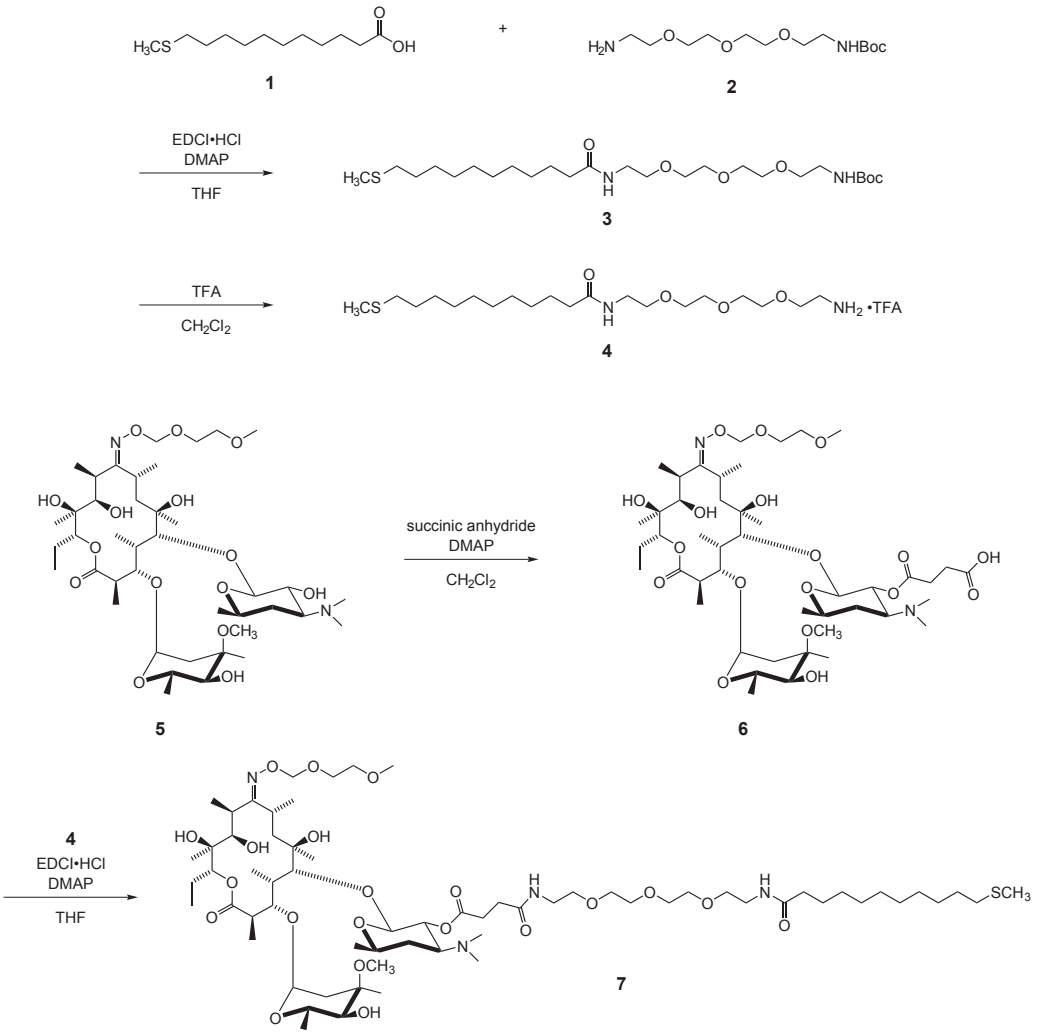

Scheme 1. Synthesis of a RXM derivative that forms SAM on the gold surface.

structure elucidation, a methylthiol unit (**3**) was generated by coupling of compounds **1** and **2** with EDCI·HCl and DMAP in THF. After treating **3** with TFA in CH_2Cl_2, the resulting compound **4** was finally coupled with compound **6**, EDCI HCl and DMAP in THF to give the RXM derivative (**7**) that forms SAM on the gold electrode surface (Scheme 1).

2.2. Biochemistry and bioinformatics

2.2.1. Microplate-based T7 phage display (T7PD) biopanning

We used a T7 phage-based cloning system to screen for RXM-binding peptides. The T7 phage libraries were constructed from cDNA of human leukocytes or Drosophila KC cells. In addition to the advantages for facile preparation of cDNA, Drosophila is a biomaterial commonly used in embryogenic studies including angiogenesis [35,36]. Each T7 phage library was applied onto streptavidin-coated wells bearing an immobilized bio-RXM (Fig. 1). Effective biopanning conditions were explored by repeated rounds of selection using various wash and elution buffers. Although no T7 phage particles were enriched by the use of the human leukocyte T7 phage library, a monoclonal T7 phage that potentially recognizes RXM was identified from the Drosophila T7 phage library. As shown in Fig. 2A, the ratio of rescued phage titer against input titer on round 4 was almost 3.5-fold, which was 1.9- or 15.2-fold higher than that from the linker-immobilized well and non-immobilized control well, respectively (Fig. 2B). T7 phage clones after the fourth round of selection were arbitrarily sampled from the eluate. The phage DNA sequence encoding the displayed peptide from each clone was then sequenced. Of the 18 monoclonal T7 phage clones analyzed, the most enriched clones (7/18) were found to display a polypeptide of 131 amino acids (Fig. 2C, Table S1).

2.2.2. Retrieval of human proteins that have similarity to the 131-mer polypeptide

A FASTA3 search using the RXM-recognizing 131-mer amino acid sequence as a query identified a number of potential hits (Fig. S1). Interestingly, the sequence of the 131-mer polypeptide corresponded to a portion of a Drosophila CG6192 protein (907 amino acids), which is a membrane-associated protein of unknown function that potentially binds calcium. Despite its origin from Drosophila, the CG6192 protein displays sequence similarity to the extracellular domain (BIG3, E458–T596) of mouse and human Angiomotin (Amot) (Fig. 2C, Fig. S1). Amot is a membrane-associated receptor found on the surface of blood endothelial cells and was identified as a receptor of angiostatin (Anst), an endogenous circulating angiogenesis inhibitor of a proteolytically

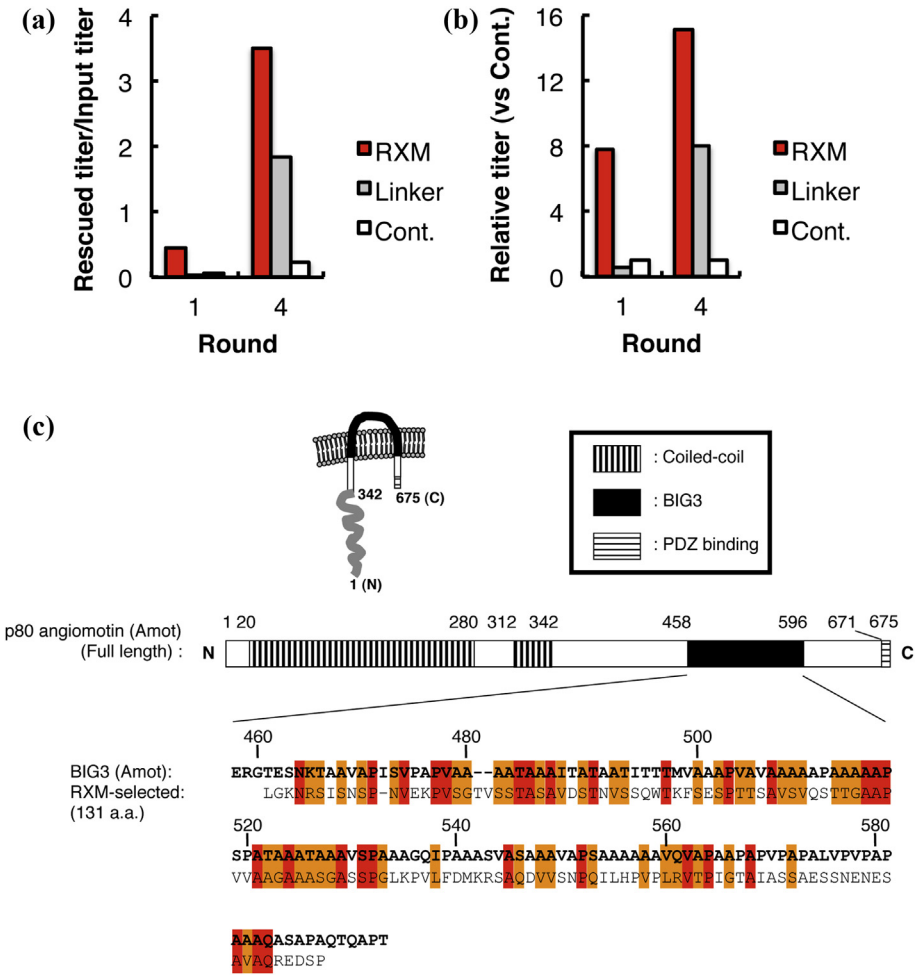

Fig. 2. Biopanning of RXM-recognizing protein by microplate-based T7 phage display. A: Enrichment of the population of T7 phages by biopanning for RXM. The bio-RXM or biotin linker immobilized well was allowed to react with the T7 phage library for 3 h at room temperature. After washing the well, remaining T7 phage was recovered, plated and incubated with host *E. coli* to form T7 phage plaques. The titer was calculated by plaque counting. A non-bio-RXM immobilized well was used as a control. B: Relative phage titer (pfu) from the eluted fraction (*vs* control). C: Schematic representation of Amot receptor and similarity of amino acid sequence between the RXM-selected 131-mer polypeptide and the extracellular BIG3 domain (E458–T596) on Amot. Residues exhibiting identity are highlighted in red, similarity are in orange.

derived fragment of plasminogen [30]. Amot is known to regulate vascular endothelial cell–cell junctions and cell motility [28–31]. Anst binds to Amot *via* its extracellular domain (BIG3, E458–T596) and inhibits endothelial cell migration and proliferation, thereby inhibiting primary tumor growth and angiogenesis-dependent growth of metastases [37–39]. In addition, Anst inhibits activation and migration of neutrophils that express Amot [32,33]. Furthermore, recent studies have demonstrated that therapeutic antibodies and DNA vaccines targeting Amot inhibit FGF-2 and VEGF-induced endothelial cell migration, resulting in an inhibition of pathological blood vessel formation associated with tumor growth [40–42]. Intriguingly, these biological effects elicited by the Amot antibodies are consistent with those of RXM *in vivo* [3–9,11], suggesting that RXM may interact with Amot to inhibit tumor angiogenesis and metastasis, as is the case for Anst or Amot antibodies.

2.2.3. QCM-D or QCM biosensor-based one-cycle T7PD biopanning

Besides their preferential affinity for small molecules, T7 phage clones are often enriched as false positives using conventional microplate-based T7PD. The relatively high incidence of false positives could be due to nonspecific binding of capsid or other proteins of the T7 phage to the avidin-coated microplate. Alternatively, some phage clones may display favorable growth properties during the amplification process, which largely depend on the physicochemical properties or molecular size of the fusion protein displayed on the phage capsid. To reduce the number of false positives from microplate-based biopanning, we carried out a one-cycle selection of a library of T7 phage-displayed short random peptides. Two different types of QCM biosensor were employed; a quartz-crystal microbalance with dissipation monitoring system (QCM-D) of flow injection type (Qsense, Meiwafosis) [24,25], or a cuvette-type QCM apparatus (AffinixQ, Initium) [15]. Fig. 3A shows representative frequency (Δf) and dissipation shifts (ΔD) during a panning process employing the QCM-D system (Qsense, Meiwafosis). The 65-MHz QCM frequency on overtone measurement decreased approximately 40 Hz on average 10 min after the injection of T7 phage library. After rinsing the flow cell to remove unbound T7 phage, the flow cell was filled with *Escherichia coli* culture and left for 15 min to promote infection by the bound T7 phage particles. This phage recovery process was repeated twice, and the resulting solution was fractionated. Fig. 3B shows D-f plots for the

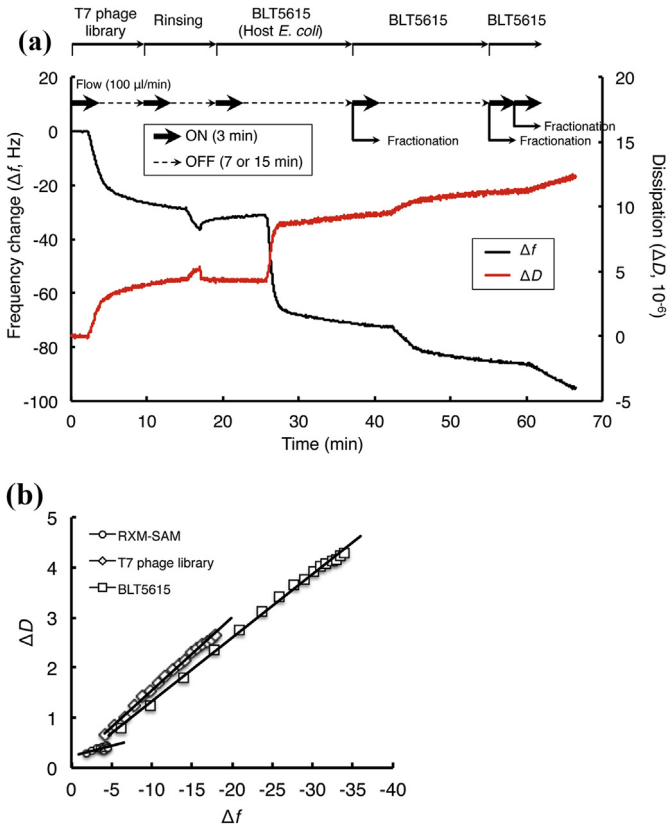

Fig. 3. Biopanning using a QCM-D biosensor. A: Representative sensorgram on QCM-D during biopanning of a T7 phage-displayed 15-mer random peptide library. The 65-MHz sensor of frequency change (Δf) and dissipation (ΔD) on overtone measurement is represented. B: D–f plot of each process.

first 2 min when the sensors started shifting in each process. The resulting apparent $\Delta D/\Delta f$ ratio, induced energy loss per unit coupled mass, was -0.146×10^{-6} Hz^{-1} after T7 phage library injection, which was over 3-fold bigger than that for RXM-SAM (-0.042×10^{-6} Hz^{-1}). This observation indicates the coverage of electrode surface by T7 phage particles (MW: ~45 MDa, ~100 nm in height) [12,15] is much more dissipative compared to the RXM-SAM (MW: 1325.8, ~4 nm in height) [24,25]. The apparent $\Delta D/\Delta f$ ratio during host BLT5615 *E. coli* culture injection was -0.127×10^{-6} Hz^{-1}, almost the same as that of T7 phage library in this experiment. Although the Sauerbrey equation was not applicable for biopanning on this QCM-D apparatus [25], these apparent parameters can be utilized as an indicator of each biopanning process. The T7 phage clones were arbitrarily sampled from the fractionated solution and sequenced. In total, 92 of the RXM-recognizing short peptides were determined (Table S4). The information content within this subset of peptides, or similarity with the amino acid sequence of Amot, was then analyzed using the RELIC program as described later.

Collection of another subset of RXM-recognizing peptides was also carried out using a cuvette-type QCM apparatus (AffinixQ, Initium) as reported previously [15,20,26,34]. The QCM sensor chip, whose gold electrode surface was covered with RXM (or Anst as a control), was immersed into a buffer-filled cuvette and the sensor allowed to stabilize. A random peptide T7 phage library was then injected into the cuvette and binding of T7 phages were monitored for 10 min (Fig. S3A, B). The RXM-binding T7 phage DNA was recovered and sequenced according to our previous report [15]. In this screen, 25 RXM-recognizing peptides (Table S5) and 59 Anst-recognizing peptides as a control (Table S6) were identified.

2.2.4. Bioinformatics analysis using the RELIC program

To evaluate the peptide sequences selected by one-cycle biopanning on the QCM biosensor and the likely binding of RXM to Amot, bioinformatics analysis of RXM-selected peptides was conducted using MOTIF1 and INFO programs in RELIC [13,43]. Analysis of the RXM- or Anst-selected peptides (Tables S4–6) using RELIC/MOTIF 1 program identified five-continuous motifs that are conserved in each peptide group (Tables S7–9), indicating the increase in information content for RXM or Anst recognition within the amino acid sequence of the selected peptides. Furthermore, RELIC/INFO analysis using each subset of peptides (Tables S4–6) also indicated that curves of information content (Fig. 4, solid line) showed an upward shift as compared with the unselected parent library (dotted line) (Tables S10–13).

To verify the likely binding interaction between RXM and Amot,

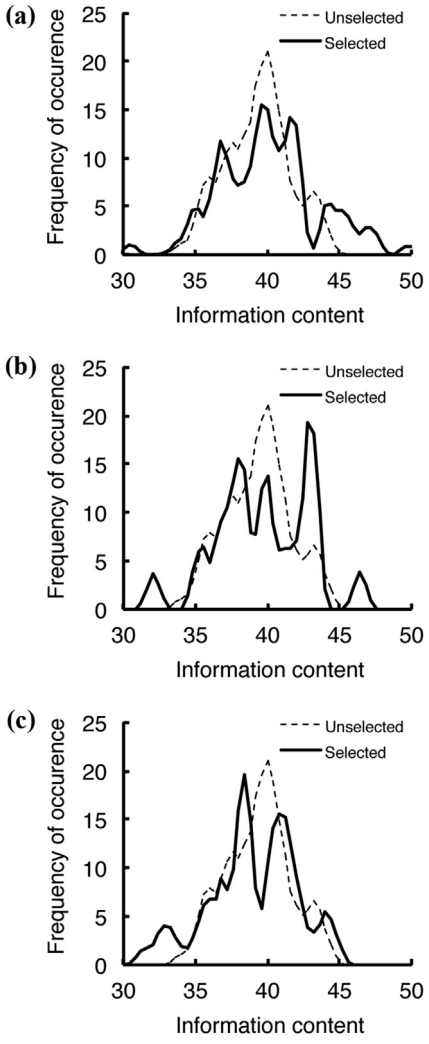

Fig. 4. Shift in the information profile of the 15-mer random peptide library following biopanning against RXM or Anst. A: 92 of RXM-selected peptides (Tables S4 and S11) on a flow injection-type QCM-D biosensor. B: 25 of RXM-selected peptides (Tables S5 and S12) on a cuvette-type QCM biosensor. C: 59 of Anst-selected peptides (Tables S6, S13) on a cuvette-type QCM biosensor. The dotted line represents the information profile of 103 arbitrarily selected peptides taken from the unscreened parent T7 phage-displayed library (Tables S2 and S10).

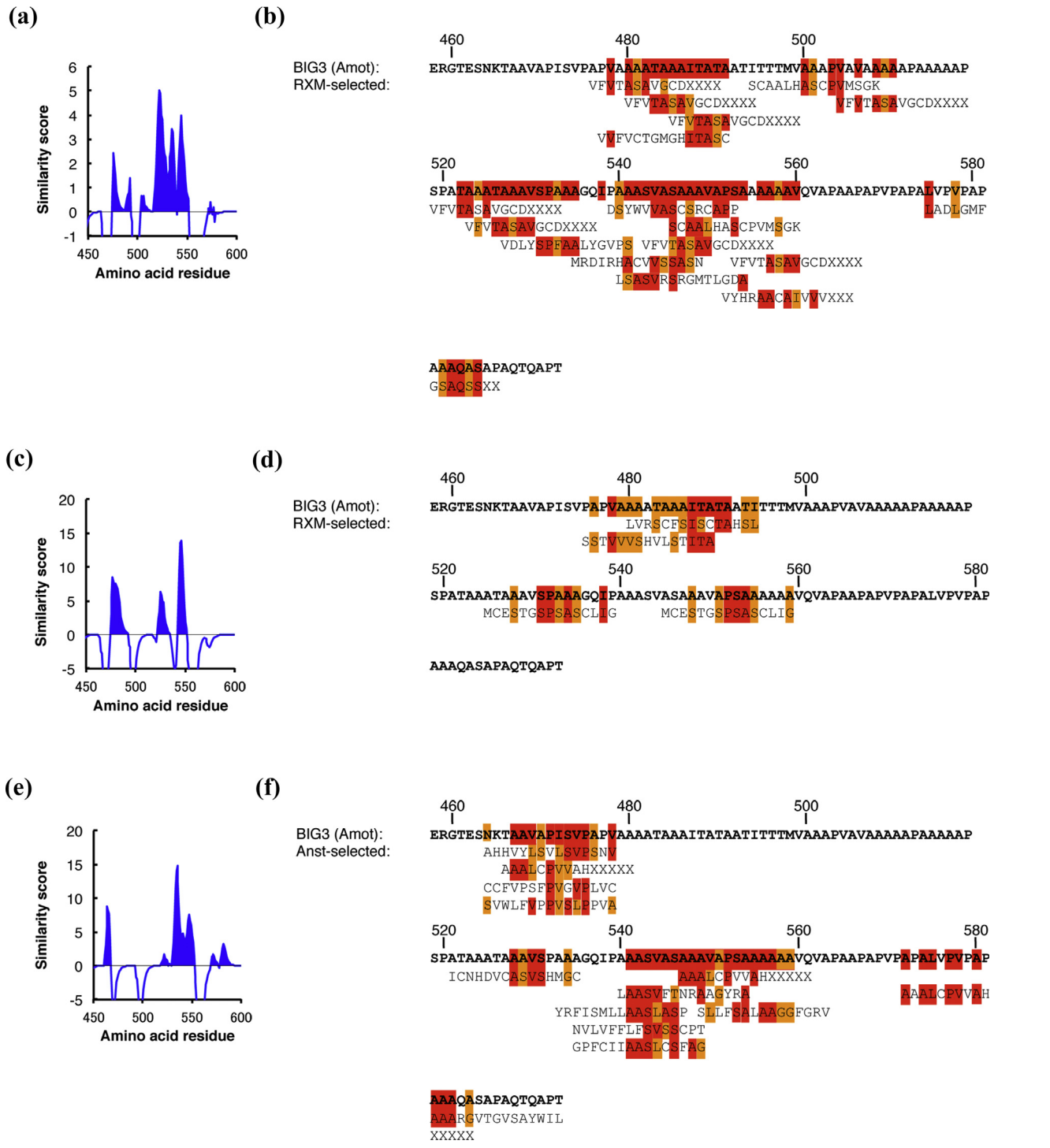

Fig. 5. Analysis of the similarity of amino acid sequence between RXM- or Anst-selected peptides and BIG3 domain in p80 Amot using RELIC/MATCH program. A, C, E: Similarity plots. Scores for the sequence of p80 Amot (M1-I675) against the sequences of 92 (A) or 25 (C) of the RXM-selected peptides, or 59 of the Anst-selected (E) peptides were calculated. The similarity scores of 103 random-peptides chosen without affinity selection (Table S2) and 27 of the control peptides recognizing the gold electrode surface (Table S3) were subtracted from these scores to remove library bias and background noise. B, D, F Cluster diagrams. A highlighted mapping of amino acid sequence between 92 (B) or 25 (D) of the RXM-selected peptides, or 59 of the Anst-selected (F) peptides and extracellular domain (BIG3, E458-T596) in Amot. Residues exhibiting identity are highlighted in red; similarity in orange. X denotes any of the 20 standard amino acids.

similarity of the amino acid sequence between RXM-selected short peptides and Amot p80 was investigated by the RELIC/MATCH program according to the previous reports [13,15,20,26]. Fig. 5 represents similarity plots (Fig. 5A, C) and cluster diagrams of the amino acid sequence (Fig. 5B, D) between RXM-selected peptides and amino acid sequence of the extracellular domain (BIG3, E458–T596) on Amot. The RXM-recognizing peptides from QCM biosensor-based selection of both the flow injection and cuvette-type platforms gave positive scores to the extracellular domain, suggesting that RXM binds to this region in agreement with the

results from our microplate-based biopanning (Fig. 2C). In particular, mainly two regions of amino acid sequence, A476–A510 and A521–V562, which might comprise alpha helices (Fig. S4), were commonly highlighted by the RXM-selected peptides from both screening platforms (Fig. 5B, D). These observations indicate that the corresponding portions of amino acid sequence sterically comprise RXM-binding site within the BIG3 domain. Furthermore, as expected, a subset of control peptides that recognize Anst (Table S6), a known protein binder of Amot, also showed a similarity with the extracellular domain on Amot (Fig. 5E, F), supporting the accuracy and reliability of this approach. The highlighted region A521–V562 (Fig. 5F) of the potential Anst binding site was common with that of RXM (Fig. 5B, D). By contrast, the N464–V478 sequence, another Anst contact region of a potential coiled domain on the N-terminus of the A476–A510 alpha helix (Fig. S4), was specifically highlighted in the analysis using Anst-selected

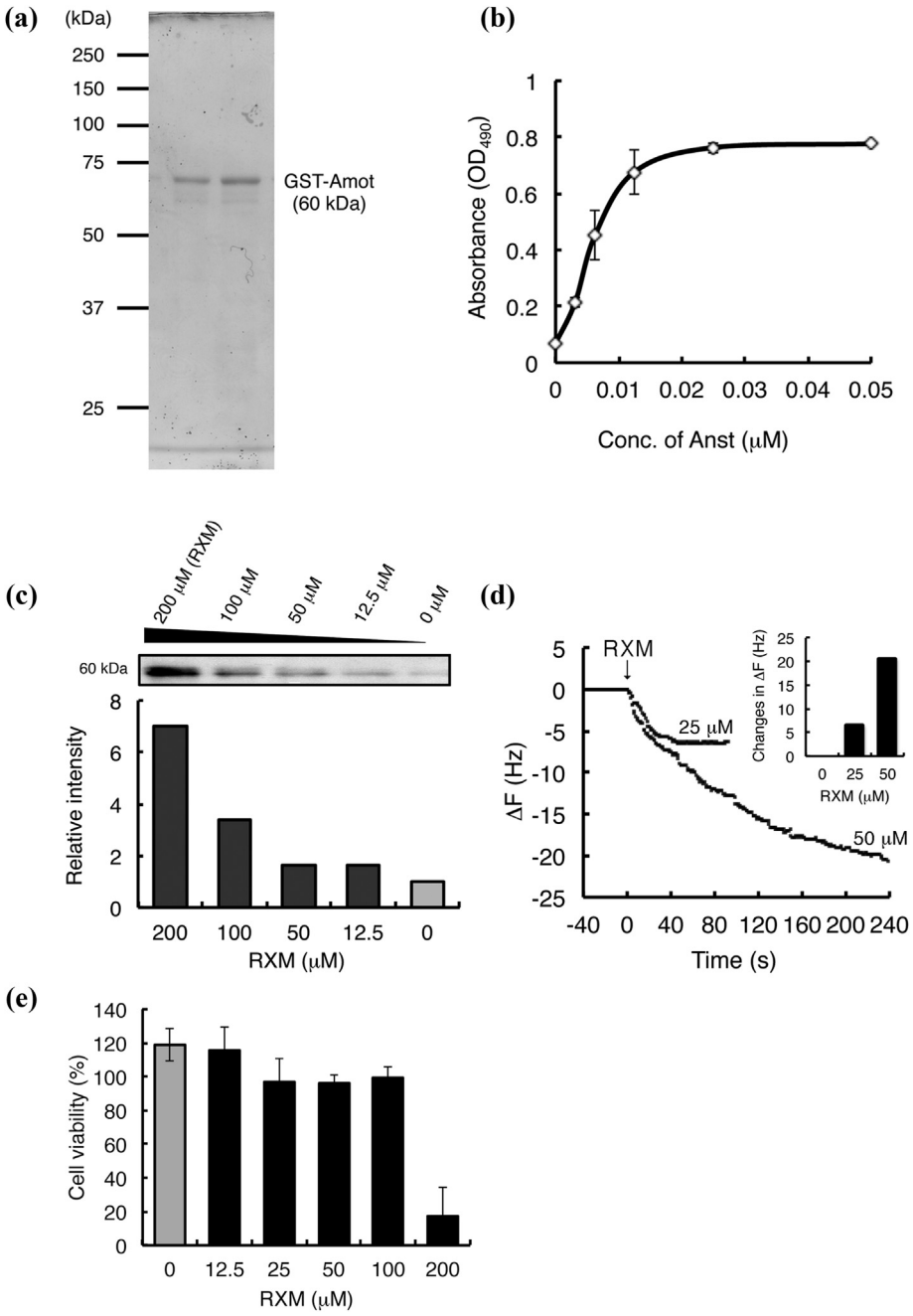

Fig. 6. Interaction between RXM and a recombinant GST tagged form of Amot (H343–I675). A: Detection of GST-Amot protein (60 kDa) after purification by affinity chromatography. Fractions were analyzed *via* SDS-PAGE and subsequent CBB staining. B: Verification of binding ability of GST-Amot with Anst by ELISA. The data are means of two independent experiments. The K_D value was estimated to be 3–6 nM, which was consistent with the half-maximal inhibitory activity of Anst (200 ng/ml; 5.3 nM) in the endothelial cell proliferation assay. C: Detection of the interaction between GST-Amot and bio-RXM immobilized on avidin-agarose beads. The band of GST-Amot was detected by immunoblotting using rabbit anti-GST antibody as a primary and anti-rabbit IgG antibody AP-conjugate as a secondary antibody. The band was detected using BCIP/NBT solution. Intensity of GST protein fragment on each lane was subtracted from those of GST-Amot as a background (bar graph). D: Detection of the binding of free RXM to GST-Amot immobilized on the gold electrode of QCM sensor chip. 1 Hz = 30 pg. E: Inhibition of endothelial cell proliferation by RXM on MTS assay. Data are means ± SE ($n = 3$).

peptides. This result may reflect a divergent mode of binding between Amot and RXM derived from the difference in molecular size between the two ligands.

2.2.5. Interaction between RXM and Amot in the bead pull down and QCM biosensor-based assays

To investigate the binding affinity of RXM for Amot, a truncated GST-tagged form of Amot p80 (H343–I675, 60 kDa) was engineered for expression in *E. coli* and the recombinant protein was purified (Fig. 6A). As shown in Fig. 6B, the GST-fused truncated Amot (GST-Amot), which contains the Anst binding region (E458–T596), retained the binding ability with Anst. The K_D value between GST-Amot and Anst was estimated to be 3–6 nM, which was consistent with the half-maximal inhibitory activity of Anst (200 ng/ml; 5.3 nM) in the endothelial cell proliferation assay [39]. In the pull down assay, RXM, fixed on avidin beads, recruited the solubilized truncated GST-Amot in a concentration-dependent manner (Fig. 6C), demonstrating that RXM directly interacts with Amot. Because full length Amot (Amot p80) is membrane-associated and potentially unstable in a small-molecule pull down assay, the band was not detected from a HUVEC cell extract. Interaction between RXM and GST-Amot was further confirmed using a QCM biosensor-based assay. Unlike the pull down assay, the recombinant Amot was in turn fixed onto the gold electrode of the QCM sensor chip and non-biotinylated free RXM was injected into the buffer-filled cuvette where the Amot-immobilized sensor chip was immersed. Fig. 6D shows the QCM sensorgram after RXM injection into the cuvette. A frequency decrease was clearly observed after injection of 25 or 50 mM of RXM (final concentration: 25 or 50 μM, respectively), which was not observed for the control, demonstrating the binding affinity of RXM for Amot. Furthermore, it was found that the biotin linker introduced at position 6 in the macrolide sugar of RXM (Fig. 1) does not interfere with the interaction with Amot. Unfortunately, injection of higher concentrations of RXM was not possible due to its limited solubility, which precluded any kinetic analysis using this system. Nevertheless, the IC_{50} of RXM for HUVEC was determined to be 100–200 μM on an MTS assay (Fig. 6E). This finding is consistent with the result of our binding assays (Fig. 6C, D) and indicates that, like Anst, binding of RXM to Amot may inhibit endothelial cell proliferation and lead to angiogenesis. However, the activity of RXM was considerably weaker (c.a. 3.3×10^4 fold) than that of Anst [39].

3. Discussion

The utility of phage display technology for target identification of bioactive small-molecules has been demonstrated [12]. However, because of some technical drawbacks, such as non-specific binding of phage particles, or phage distribution bias during the amplification process, successful examples of this technology have been somewhat limited. In the present study, we used both T7 phage-displayed protein and random peptide libraries to identify a likely binding partner for the anti-angiogenic macrolide RXM. Subsequent analysis of our biopanning hits with a range of bioinformatics tools allowed us to identify Amot as a direct binding protein.

Biopanning from a T7 phage-displayed protein library was conducted using a conventional microplate-based method with repeated rounds of selection. Small-molecules, immobilized on a microplate, generally recognize binding pockets comprised of two- or three-dimensional structures of the target protein(s) displayed on the T7 phage capsid, provided the immobilized small-molecule is accessible to the binding pocket of the larger protein [23]. In general, binding affinity of such “lock-and-key” type docking of small-molecules to proteins is stronger than to short peptides on T7 phage, which results in a clear enrichment of monoclonal T7 phage by repeated rounds of selection. Here, we identified a 131-mer polypeptide (7/18) after the fourth round of selection using bio-RXM. According to our cognate bioinformatics analysis and binding assays, this polypeptide, having a similar amino acid sequence to the extracellular domain on human Amot (Fig. 2C), seems to recognize RXM *via* part of the steric structure that is comprised of alpha helices (Figs. S4, S5).

By contrast, one-cycle biopanning of a T7 phage-displayed random peptide library has been conducted using QCM biosensors. Unlike proteins, short peptides can be readily displayed on the T7 phage capsid and contact with immobilized small-molecules *via* several amino acid residues with weak affinity (K_D:10^{-3}–10^{-4} M) can be detected. Use of a biosensor as a biopanning platform enables efficient rapid capture of such peptides displaying weak affinity without the need for repeated rounds of selection. Indeed, RXM-recognizing peptides were identified from both the flow injection- and cuvette-type of QCM biosensor. Analysis of the peptide sequences on the selected phage indicated similarity to the extracellular domain (BIG3) of Amot, suggesting the presence of an RXM-binding site. Amot is a membrane-associated receptor protein that is rich in alanine residues. As such, it might be technically challenging to investigate the precise docking manner of Amot by site-directed mutagenesis or point mutation of amino acid residues. A further advantage of our approach using QCM- or QCM-D-based methodologies is that combinatorial and high throughput discovery of other drug binding candidate proteins (e.g. proteins involved in ADMET) is feasible by using the same subset of RXM-recognizing short peptides and RELIC bioinformatics analysis. For example, in addition to Amot, RXM-selected peptides showed positive scores against liver cytochrome P450 CYP3A4, a well-known enzyme (monooxygenase) involved in the catabolism of RXM [44].

Due to a variety of biological activities, macrolides are an attractive family of compounds for use as chemotherapeutics. Indeed, RXM has been used clinically as an antibiotic for many years, thus ensuring its safe use in the treatment of humans. A further medical application of RXM comes from its ability to inhibit tumor angiogenesis and metastasis, although details of the mechanism of action have not been fully established. In this study, we have shown that RXM directly binds to Amot *via* BIG3 domain where the endogenous anti-angiogenic inhibitor Anst directly binds and inhibits tumor angiogenesis and metastasis [30,37–39]. Amot was first identified as a receptor of Anst by using a yeast two hybrid system [30]. Since then, the various roles of Amot have been extensively studied. In particular, DNA vaccines or antibodies targeting Amot have successfully demonstrated their therapeutic efficacy for tumor therapy [40–42]. Although the binding affinity of RXM for Amot is relatively weak, along with its inhibitory effect on endothelial cell proliferation (IC_{50}: 100–200 μM, Fig. 6C–E), these observations correlate with the reported weak anti-angiogenic effect of RXM *in vivo*. Our results suggest Amot could be a promising target for novel tumor chemotherapeutics. Moreover, studies into the generation of macrolide derivatives targeting Amot may lead to the development of superior anti-angiogenic compounds. To the best of our knowledge, this is the first example of small-molecule that directly binds to Amot [31].

4. Experimental section

4.1. Chemistry (general)

4.1.1. Materials

All non-aqueous reactions were carried out using freshly distilled solvents under an atmosphere of argon. All reactions were

monitored by TLC, which was carried out on Silica Gel 60 F254 plates (E. Merck, Darmstadt, Germany). Flash chromatography separations were performed on PSQ 100B (Fuji Silysia Co., Ltd, Japan).

The NMR spectra (^{1}H, ^{13}C) were determined on a Bruker 600 MHz or 400 MHz spectrometer (Avance DRX-600, Avance DRX-400) or a JEOL 400 MHz spectrometer (JNM-LD400), using $CDCl_3$ (with TMS for ^{1}H NMR and chloroform-*d* for ^{13}C NMR as the internal reference) solution, unless otherwise noted. Chemical shifts were expressed in parts per million (ppm) and coupling constants are in Hertz. Optical rotations were recorded on a JASCO P-1030 digital polarimeter using the sodium D line at room emperature, using $CHCl_3$ as a solvent unless otherwise noted. Infrared spectra (IR) were recorded on a Jasco FT/IR-410 spectrometer using NaCl (neat) or KBr pellets (solid), and were reported as wavenumbers (cm^{-1}). Mass spectra (MS) were obtained on an Applied Biosystems mass spectrometer (API QSTAR pulsar i) under conditions as high resolution, using polyethylene glycol as internal standard.

4.1.2. Synthesis of RXM derivative that forms SAM

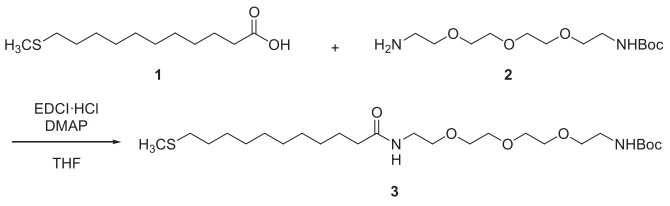

To a solution of **2** (575 mg, 1.81 mmol) in THF was added **1** followed by EDCI·HCl (347 mg, 1.81 mmol) and DMAP (15 mg, 0.12 mmol) at room temperature. The mixture was stirred at room temperature for 3 d. Then the mixture was quenched by the addition of H_2O and diluted with EtOAc. The layers ware separated, and the organic layer was washed with brine and dried with Na_2SO_4. After the organic layer was concentrated, the residue was purified by silica gel chromatography ($CHCl_3$/MeOH = 50/1) to yield **3** (426 mg, 69%) as a colorless oil. ^{1}H NMR (400 MHz, $CDCl_3$) δ 6.12 (1H, *br* s), 5.09 (1H, *br* s), 3.66–3.60 (8H, m), 3.56–3.53 (4H, m), 3.47–3.42 (2H, m), 3.34–3.28 (2H, m), 2.48 (2H, t, *J* = 7.4 Hz), 2.17 (2H, t, *J* = 7.6 Hz), 2.09 (3H, s), 1.66–1.54 (4H, m), 1.44 (9H, s), 1.38–1.34 (2H, m), 1.27 (10H, *br* s); ^{13}C NMR (100 MHz, $CDCl_3$) δ 173.1, 155.9, 70.39 (×2), 70.12 (×4), 69.93, 40.27, 39.01, 36.61, 34.20, 29.37, 29.32, 29.26, 29.23, 29.12, 29.09, 28.71, 28.34 (×3), 25.64, 15.44; IR (film) ν_{max} 3319, 2854, 1711, 1649, 1529 cm^{-1}; HRMS (ESI) calcd for $C_{25}H_{50}N_2O_6NaS$ $[M + Na]^+$: 529.3281, found: 529.3270.

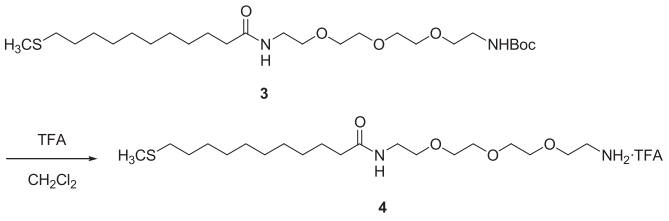

To a solution of **3** (100 mg, 0.20 mmol) in CH_2Cl_2 (2.0 ml) was added TFA (0.54 ml). The mixture was stirred at room temperature for 3.5 h and then concentrated. The resulting amine salt was purified by silica gel chromatography ($CHCl_3$/MeOH = 9/1) to yield **4** (80 mg, 77%) as a yellow oil. ^{1}H NMR (400 MHz, $CDCl_3$) δ 8.22 (2H, *br* s), 6.94 (1H, *br* s), 3.80–3.78 (2H, m), 3.69–3.68 (2H, m), 3.62–3.60 (6H, m), 3.55 (2H, t, *J* = 4.9 Hz), 3.40–3.39 (2H, m), 3.16 (2H, *br* s), 2.48 (2H, t, *J* = 7.4 Hz), 2.18 (2H, t, *J* = 7.6 Hz), 2.09 (3H, s), 1.62–1.54 (4H, m), 1.38–1.35 (2H, m), 1.27 (10H, *br* s); ^{13}C NMR (100 MHz, $CDCl_3$) δ 174.4, 70.01, 69.93, 69.89, 69.81, 69.63, 66.77, 39.46, 39.08, 36.36, 34.23, 29.41, 29.37, 29.28, 29.18, 29.15, 29.10, 28.72, 25.69, 15.44; IR (film) ν_{max} 3300, 3082, 2856, 1679, 1643, 1550, 1428 cm^{-1}; HRMS (ESI) calcd for $C_{20}H_{43}N_2O_4S$ $[M\text{-}CF_3CO_2]^+$: 407.2938, found: 407.2930.

To a solution of **5** (800 mg, 0.95 mmol) in CH_2Cl_2 (4.0 ml) was added succinic anhydride (114 mg, 1.14 mmol) followed by DMAP (12 mg, 0.10 mmol) at room temperature. The mixture was stirred at room temperature for 3 d. Then the mixture was quenched by the addition of H_2O and diluted with EtOAc. The layers ware separated, and the organic layer was washed with brine and dried with Na_2SO_4. After the organic layer was concentrated, the residue was purified by silica gel chromatography ($CHCl_3$/MeOH = 5/1) to yield **6** (579 mg, 65%) as a white solid. $[\alpha]_D$ −86.0 (*c* = 0.9 in $CHCl_3$); ^{1}H NMR (400 MHz, $CDCl_3$) δ 5.17 (2H, s), 5.10 (1H, dd), 4.93–4.90 (1H, m), 4.64 (1H,d, *J* = 7.4 Hz), 4.32 (1H, *br* s), 3.96–3.93 (1H, m), 3.91 (1H, d, *J* = 10 Hz), 3.79–3.71 (4H, m), 3.57–3.56 (3H, m), 3.49 (1H, d, *J* = 6.8 Hz), 3.41 (3H, s), 3.36 (3H, s), 3.16 (1H, *br* s), 3.20–3.08 (1H, m), 3.04 (1H, d, *J* = 9.6 Hz), 2.90–2.80 (1H, m), 2.70–2.63 (6H, m), 2.50 (6H, s), 2.42 (1H, s), 2.34 (1H, d, *J* = 15 Hz), 2.17 (1H, *br* s), 1.97–1.86 (3H, m), 1.61 (1H, dd, *J* = 5.0 Hz), 1.47 (3H, s), 1.45–1.39 (3H, m), 1.29–1.15 (19H, m), 1.04 (3H, d, *J* = 7.2 Hz), 0.89 (3H, d, *J* = 7.8 Hz), 0.83 (3H, t, *J* = 7.2 Hz); ^{13}C NMR (100 MHz, $CDCl_3$) δ 176.7, 174.9, 172.7, 172.1, 100.0, 97.43, 96.01, 84.01, 80.04, 77.78, 76.68, 74.66, 74.20, 72.90, 71.82, 70.37, 70.12, 68.30, 67.39, 65.79, 63.11, 59.04, 49.40, 44.73, 39.22 (×2) 38.59, 36.96, 35.08, 33.07, 31.46, 31.16, 29.25, 26.86,

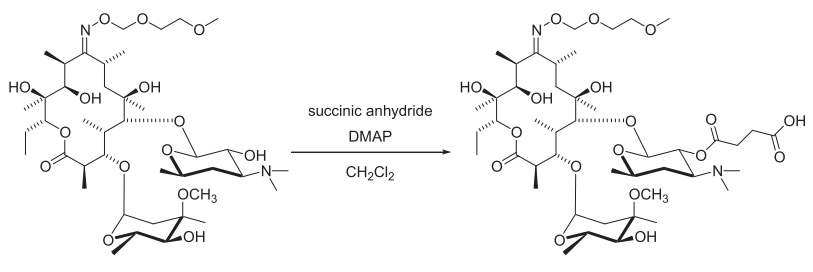

21.48 (×2), 21.25, 21.08, 18.60, 18.46, 16.47, 16.19, 14.74, 10.55, 9.19; IR (film) ν_{max} 3427, 1737, 1575, 1462, 1377, 1167 cm^{-1}; HRMS (ESI) calcd for $C_{45}H_{80}N_2O_{18}Na$ $[M + Na]^+$: 959.5298, found: 959.5255.

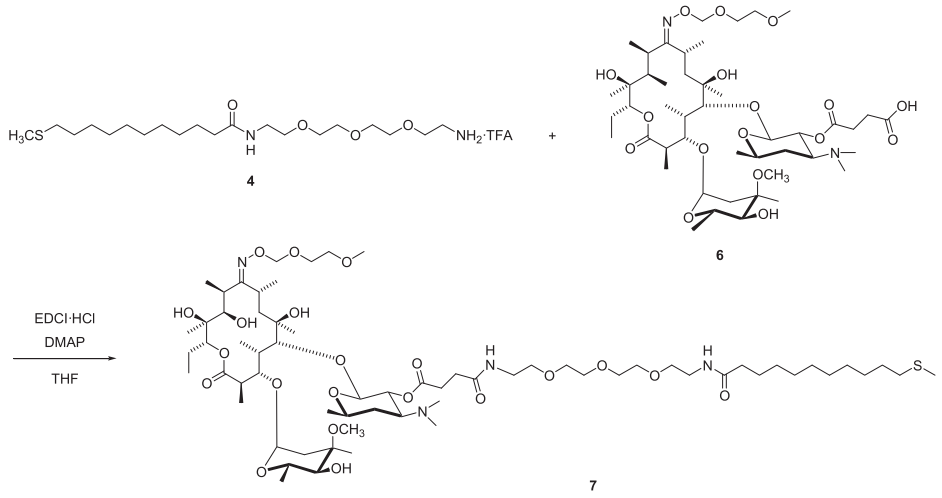

To a solution of **4** (76 mg, 0.15 mmol) in THF (3 ml) was added **6** (145 mg, 0.15 mmol) followed by EDCI·HCl (57 mg, 0.30 mmol) and DMAP (5.5 mg, 0.05 mmol) at room temperature. The mixture was stirred at room temperature for 24 h. Then the mixture was quenched by the addition of H_2O and diluted with EtOAc. The layers were separated, and the organic layer was washed with brine and dried with Na_2SO_4. After the organic layer was concentrated, the residue was purified by silica gel chromatography ($CHCl_3$/MeOH = 29/1 to 9/1) to yield **7** (99 mg, 50%) as a white amorphous solid. $[\alpha]_D$ −57.0 (c = 1.0 in $CHCl_3$); ^1H NMR (400 MHz, $CDCl_3$) δ 6.47 (1H, *br* s), 6.17 (1H, br s), 5.17 (2H, s), 5.09 (1H, dd, J = 2.0 Hz), 4.88 (1H, d, J = 4.6 Hz), 4.74 (1H, dd, J = 7.4 Hz), 4.57 (1H, d, J = 7.6 Hz), 4.33 (1H, s), 4.02–3.99 (1H, m), 3.94 (1H, d, J = 9.5 Hz), 3.81 (1H, s), 3.78–3.71 (3H, m), 3.65 (8H, *br* s), 3.56 (7H, *br* s), 3.47-3.45 (6H, m), 3.41 (3H, s), 3.34 (3H, s), 3.17 (1H, s), 3.03 (1H, t, J = 9.5 Hz), 2.89–2.85 (1H, m), 2.67–2.62 (5H, m), 2.52–2.48 (3H, m), 2.40 (1H, d, J = 11 Hz), 2.32 (1H, t, J = 9.9 Hz), 2.23 (6H, *br* s), 2.17 (2H, t, J = 7.7 Hz), 2.10 (3H, s), 1.95–1.93 (2H, m), 1.70 (1H, d, 12 Hz), 1.62–1.55 (7H, m), 1.48–1.45 (4H, m), 1.35 (2H, t, J = 8.5 Hz), 1.27–1.15 (29H, m), 1.04 (3H, d, J = 6.8 Hz), 0.91 (3H, d, J = 7.6 Hz), 0.83 (3H, t, J = 7.3 Hz); ^{13}C NMR (100 MHz, $CDCl_3$) δ 175.1, 173.2, 172.7, 171.8, 171.6, 100.8, 97.40, 96.11, 84.00, 80.05, 78.02, 77.32, 76.83, 74.77, 74.25, 72.81, 71.94, 71.85, 70.46, 70.38, 70.21, 70.15, 69.99 (×2), 69.91, 68.29, 65.54, 63.91, 59.08, 49.45, 44.70, 40.72, 39.38 (×2), 39.10, 38.87, 37.15, 36.70, 35.06, 34.29, 33.08, 31.44, 30.36, 29.86, 29.47, 29.42, 29.36, 29.33, 29.22, 29.17, 28.80, 26.95, 26.85, 25.73, 21.53, 21.23, 21.18, 18.63, 18.53, 16.46, 16.13, 15.53, 14.77, 10.61, 9.17; IR (film) ν_{max} 3340, 2969, 2927, 2876, 2857, 1735, 1650, 1547, 1455, 1375, 1346, 1275 cm^{-1}; HRMS (ESI) calcd for $C_{65}H_{121}N_4O_{21}S$ $[M + H]^+$: 1325.8238, found: 1325.8256.

4.2. Biochemistry

4.2.1. Materials

DMEM was purchased from Nacalai Tesque Co. Ltd (Kyoto, Japan). Endothelial cell growth media kits were obtained from Lonza Japan Inc. (Tokyo, Japan). Cloning System was obtained from Novagen (Madison, WI). The GSTrap FF column and Glutathione Sepharose™ 4B were purchased from GE Healthcare (Amersham, UK). RNA extraction reagent (Sepasol-RNA Super G) was from Nacalai Tesque Co. Ltd. Restriction enzymes *Eco*RI and *Xho*I were obtained from TOYOBO (Osaka, Japan). T4 DNA ligase was from Promega (Madison, WI). PCR reagent was obtained from TaKaRa (Tokyo, Japan). Avidin-agarose bead was from Sigma–Aldrich (St Louis, MO). A rabbit anti-mouse IgG antibody AP conjugate was obtained from Cell Signaling Technology Inc. (Danvers, MA, USA). Human angiostatin (Anst) protein (Kringles 1–4) was purchased from Alpha Diagnostic International Inc. (San Antonio, TX).

4.2.2. Cell culture

MCF-7 cells were cultured in DMEM supplemented with 10% fetal calf serum (Thermo Scientific, Rockford, IL). HUVEC cells were cultured in EBM™-2 medium (Lonza) supplemented with serum, growth factors and antibiotics. The cells were cultured in 75 cm^2 normal (MCF-7) or collagen-coated (HUVEC) flasks at 37 °C in a humidified chamber containing 5% CO_2. The culture medium was changed every second day.

4.2.3. MTS assay

Cell proliferation was evaluated using a colorimetric [3-(4,5-dimethylthazol-2-yl)-5-(3-carboxy-methoxyphenyl)-2-(4-sulfophenyl)-2H-tetrazolium, inner salt] (MTS) assay (Promega). The cells (5×10^3 cells) were plated in 96-well plates and incubated with various concentrations (12.5–200 μM, final) of RXM for 72 h at 37 °C/5% CO_2. A 20 μL aliquot of MTS reagent was added to each test well followed by an additional incubation at 37 °C/5% CO_2 for 60 min. Cell proliferation was determined by measuring optical density at 490 nm.

4.2.4. Microplate-based biopanning

Biotinylated RXM derivative was immobilized on a streptavidin-coated 96-well microplate at 4 °C, O/N. The wells were then blocked with 3% skimmed milk in 100 mM Tris–HCl (pH 8.0) for 1 h. An aliquot (1.0×10^9 pfu/100 μl) of the library of T7 phage was allowed to bind to the RXM for 3 h. After washing ten times with 200 μL of 100 mM Tris–HCl (pH 7.5) (every 5 min on shaker), 150 mM NaCl to remove non-specifically bound phage, the remaining phage particles were rescued using 100 mM Tris–HCl (pH 7.5), 150 mM NaCl and 3% Tween20 at room temperature for 90 min. Following four rounds of selection, the recovered phage solution was diluted, mixed with 200 μl of log-phase host *E. coli* (BLT5615) solution (cultured in the presence of 50 μg/ml of carbenicillin until OD_{600} of

1.0 and then incubated for 30 min with 1 mM of IPTG) and 4 ml of pre-warmed top agarose, and then plated to allow the formation of phage plaques by incubation at 37 °C for 3 h. The 28 plaques were randomly picked from LB plates and each was dissolved in 200 μl of phage extraction buffer (20 mM Tris–HCl, pH 8.0, 100 mM NaCl, 6 mM $MgSO_4$). A specific region of the T7 phage DNA was amplified by PCR using the primer pair 5′-TGCTAACTTCCAAGCGGACC-3′ (forward) and 5′-AAAAACCCCTCAAGACCCGTTTA-3′ (reverse). The amplified product was then analyzed by agarose gel electrophoresis. A 5 μl aliquot of PCR product was treated with 2 μl of ExoSAP-IT (digested at 37 °C for 15 min, then inactivated at 80 °C for 15 min) and precipitated by addition of 70% EtOH. The products were then sequenced using an ABI Prism BigDye Terminator Cycle Sequencing Kit on an ABI Prism3100 Genetic Analyzer (ABI) according to the manufacturer's protocol.

4.2.5. QCM biosensor-based biopanning

4.2.5.1. Flow injection-type QCM-D biosensor. A flow injection type of quartz-crystal microbalance fitted with a dissipation monitoring system (QCM-D) (Qsense, Meiwafosis) was used for biopanning [24,25]. The gold QCM-D sensor chip (4.95 MHz, AT cut, 14 mm in i.d., 0.3 mm thickness) was attached to an oscillator maintained at 37 °C. The flow path was filled with phage extraction buffer at a flow rate of 100 μl/min for 3 min. After rinsing the flow path with 300 μl of 70% EtOH, a solution of RXM derivative (1 mM in 70% EtOH) that forms SAM on the gold electrode was injected at the same flow rate. The frequency (Δf) and dissipation (ΔD) changes were then monitored for 3 min (Fig. S3). The flow path was again flushed with phage extraction buffer. A 300 μl aliquot of T7 phage library (15 mer, 1.0×10^8 pfu/ml in phage extraction buffer) was then injected at a flow rate of 100 μl/min, and the frequency and dissipation changes were monitored. In addition, the phage library was incubated in the flow path for 7 min to enhance the T7 phage/RXM interaction. After washing the flow path with 300 μl of phage extraction buffer to remove unbound T7 phage particles, a 300 μl aliquot of host *E. coli* (BLT5615) culture was injected and incubated for 15 min to allow infection with bound T7 phage. The host culture incubation was repeated twice more, and the resulting mixture was fractionated, and plated to facilitate isolation of selected phage. The amino acid sequence of the peptide on the selected T7 phage was then determined.

4.2.5.2. Cuvette-type QCM biosensor. Anst- or RXM-recognizing peptides (15-mer) were selected using a 27-MHz cuvette type QCM apparatus (AffinixQ, Initium) according to our original protocol [15].

4.2.6. Expression of recombinant protein using an E. coli cloning system

The H343–I675 fragment of p80 angiomotin (Amot) gene was isolated from a cDNA library of MCF-7 cells. Briefly, total RNA was extracted using Sepasol-RNA Super G (Nacalai Tesque) and then reverse transcription was performed using a ReverTra Ace® qPCR RT Kit (TOYOBO) with the following primer pair: forward primer, 5′-GGGAATTCCATGCCCAGATTATTGAGAAGG-3′; reverse primer, 5′-GGCTCGAGTTAGATGAGATATTCCACCATCTCTG-3′), according to the manufacture's instructions. The Amot gene was digested with *Eco*RI, *Xho*I and then inserted into the multi-cloning site of pET-42a(+) vector (Novagen). Competent *E. coli* BL21 (DE3) pLysS cells were then transformed with the expression plasmid.

Single colonies were transferred into 15 ml of LB medium containing 1% glucose, 50 μg/ml of kanamycin (Kan) and 34 μg/ml of chloramphenicol (Cm), and cultured at 37 °C, overnight. The cells were then transferred to 135 ml of LB medium containing 1% glucose, 50 μg/ml of Kan and 34 μg/ml of Cm for 3 h at 37 °C. IPTG was added to the culture medium at a final concentration of 0.1 mM and the cells were incubated for 3 h at 30 °C to induce recombinant protein expression. The cells were harvested by centrifugation at 5000 g for 10 min at 4 °C.

4.2.7. Purification of recombinant protein

The recombinant GST-Amot was purified by an affinity chromatography method using a Glutathione Sepharose resin (Amersham Pharmacia Biotech). The cell pellet (1 g) was resuspended in 50 ml of PE buffer (50 mM phosphate, 400 mM NaCl, 1 mM EDTA, 5 mM 2-mercaptoethanol, pH 7.3) and sonicated (5 × 30 s pulses on ice). A 50 μl aliquot of 0.01% NP-40 was added to the cell extract and the mixture stirred for 30 min on ice. The extract was then clarified by centrifugation at 20,400 g for 30 min at 4 °C. The resulting supernatant was incubated with 2 ml Glutathione Sepharose resin for 1 h at 4 °C with rotation. After washing the slurry with 15 ml of a washing buffer (PE buffer containing 0.01% NP-40), the resin was charged to a disposable column and washed using 15 ml of washing buffer, 50 ml washing buffer containing 2 M NaCl, and 50 ml washing buffer 2 (PE buffer containing 5 mM $MgCl_2$ and 1 mM ATP). The GST-Amot was then fractionated (1 ml per fraction) using an elution buffer (50 mM phosphate, 150 mM NaCl, 1 mM EDTA, 1 mM DTT, 0.01% NP-40, 10 mM glutathione, the reduced form, pH 8.0). The fractions containing GST-Amot were recovered and dialyzed overnight in PE buffer to eliminate the glutathione. The resulting sample was again purified by the same process as described above. The GST-Amot in each fraction was detected by SDS-PAGE using 10% separation gel and CBB staining. The fraction containing GST-Amot was concentrated using Amicon Ultra (Millipore, Billerica, MA) and then subjected to the binding assays.

4.2.8. ELISA

The purified GST-Amot (0.5 μM, 100 μl) was immobilized on an ELISA plate (Flexible Plate; BD Falcon, San Jose, CA) by rotating gently for 1 h. The wells were blocked with 200 μl of PBS containing 1% (w/v) skimmed milk for 1.5 h and then washed three times with PBS. A 100 μl aliquot of Anst protein solution (0.003, 0.06, 0.13, 0.25 and 0.05 μM) was individually associated with immobilized GST-Amot for 1 h. Nonspecifically bound proteins were removed by three washes with PBS and the remaining protein was detected using rabbit anti-Anst antibody as a primary antibody and anti-rabbit IgG HRP conjugate as a secondary antibody. After addition of *o*-phenylenediamine, the absorbance at 490 nm was measured using a spectrophotometer (NJ-2300, Inter Med, Tokyo, Japan) to detect Anst binding to the immobilized GST-Amot.

4.2.9. Pull down assay of GST-Amot protein

A 250 μl aliquot of bio-RXM solution (12.5–200 μM in 10% DMSO) was mixed with 50 μl of prewashed avidin-agarose beads (Sigma–Aldrich) and the suspension was incubated for 1 h at 4 °C with rotation. After washing three times with 300 μl of PE buffer, 250 μl of GST-Amot solution was mixed with the beads and incubated overnight at 4 °C with rotation. After washing the beads five times with PE buffer, the beads were mixed with 50 μl of SDS loading buffer (0.25 mM DTT, 0.5% SDS, 2.5% glycerol, 0.2% BPB in 20 mM Tris–HCl, pH 6.8) and incubated at 95 °C for 15 min. The resulting solution was subjected to SDS-PAGE using a 10% polyacrylamide gel. The separated proteins were blotted onto PVDF membrane and GST-Amot protein was detected by Western blot analysis using a mouse α-GST antibody (Sigma–Aldrich) as a primary antibody and rabbit anti-mouse IgG antibody-AP conjugate (Cell Signaling Technology Inc.). The signal was detected in BCIP/NBT solution.

4.3. Bioinformatics

4.3.1. Retrieval of RXM-associating protein using FASTA3

Proteins having a sequence similar to the selected polypeptide were identified using bioinformatics. Firstly, we dissected large number of proteins registered in the human proteome database. For convenience, the FASTA3 program (http://www.ebi.ac.uk/fasta33/), (Expectation upper value: 50, Matrix: BLOSAM50, Sequence range: −1, Number of Scores: 50, Number of Alignments: 50, Open gap penalty: −10, Gap extension penalty: −2) Swiss-Prot new library (version 3.4t25) and the expert protein analysis system (ExPASy) were utilized for the scanning procedure [14,45,46].

4.3.2. Analysis of affinity-selected peptide using RELIC server

Statistical analysis of RXM or Angiostatin (Anst)-selected 15-mer peptides and p80 Amot was calculated using stand-alone RELIC programs, kindly provided by Dr. Lee Makowski (Northeastern University, Boston, MA, USA) [13,47,48]. The score is calculated by a modified BLOSAM62 amino acid matrix within each window of five-amino-acids in length across the entire length of the protein sequence and then cumulatively plotted as a similarity plot [46,49]. As a background control, scores for 103 peptides arbitrarily selected from the unscreened parent T7 phage library (Table S2), and 27 of gold electrode-recognizing peptides (Table S3) were subtracted [15,20]. The mapping of the amino acid sequence was generated at the portion of maximal similarity score.

5. Conclusion

In this work, we identified the direct interaction between RXM and Amot using multimodal biopanning of T7 phage-displayed random peptides and protein libraries. This finding might explain the molecular basis underlying inhibition of tumor angiogenesis and metastasis by RXM. As such, Amot could be an attractive target for developing tumor chemotherapeutics. Furthermore, beyond technical limitations on conventional proteomics approaches, our strategy may contribute to target identification of any drug-like small-molecules of interest.

Acknowledgment

We acknowledge to Taisho Pharmaceutical Co., Ltd. (Tokyo, Japan) for providing RXM and helpful suggestions about synthesis of RXM derivative. We also thank Dr. Lee Makowski (Northeastern University, Boston, MA, USA) for providing the stand-alone type RELIC programs. This work was partly supported by JSPS KAKENHI Grant Number 19750145.

Appendix A. Supplementary data

Supplementary data related to this article can be found at http://dx.doi.org/10.1016/j.ejmech.2014.12.015.

References

[1] R.N. Jones, A.L. Barry, C. Thornsberry, Antimicrob. Agents Chemother. 24 (2) (1983) 209–215.
[2] F. Schlunzen, R. Zarivach, J. Harms, A. Bashan, A. Tocilj, R. Albrecht, A. Yonath, F. Franceschi, Nature 413 (6858) (2001) 814–821.
[3] J. Yatsunami, S. Hayashi, Anticancer Res. 21 (6B) (2001) 4253–4258.
[4] D. Aoki, S. Ueno, F. Kubo, T. Oyama, T. Sakuta, K. Matsushita, I. Maruyama, T. Aikou, Anticancer Res. 25 (1A) (2005) 133–138.
[5] T. Oyama, T. Sakuta, K. Matsushita, I. Maruyama, S. Nagaoka, M. Torii, J. Periodontol. 71 (10) (2000) 1546–1553.
[6] J. Yatsunami, N. Tsuruta, Y. Fukuno, M. Kawashima, S. Taniguchi, S. Hayashi, Clin. Exp. Metastasis 17 (2) (1999) 119–124.
[7] J. Yatsunami, Y. Fukuno, M. Nagata, M. Tominaga, S. Aoki, N. Tsuruta, M. Kawashima, S. Taniguchi, S. Hayashi, Clin. Exp. Metastasis 17 (4) (1999) 361–367.
[8] J. Yatsunami, N. Tsuruta, N. Hara, S. Hayashi, Cancer Lett. 131 (2) (1998) 137–143.
[9] J. Yatsunami, Y. Fukuno, M. Nagata, N. Tsuruta, S. Aoki, M. Tominaga, M. Kawashima, S. Taniguchi, S. Hayashi, Cancer Lett. 147 (1–2) (1999) 17–24.
[10] S. Abe, H. Nakamura, S. Inoue, H. Takeda, H. Saito, S. Kato, N. Mukaida, K. Matsushima, H. Tomoike, Am. J. Respir. Cell Mol. Biol. 22 (1) (2000) 51–60.
[11] J. Tamaoki, J. Nakata, E. Tagaya, K. Konno, Antimicrob. Agents Chemother. 40 (7) (1996) 1726–1728.
[12] Y. Takakusagi, K. Takakusagi, F. Sugawara, K. Sakaguchi, Expert Opin. Drug Discov. 5 (4) (2010) 361–389.
[13] S. Mandava, L. Makowski, S. Devarapalli, J. Uzubell, D.J. Rodi, Proteomics 4 (5) (2004) 1439–1460.
[14] W.R. Pearson, D.J. Lipman, Proc. Natl. Acad. Sci. U. S. A. 85 (8) (1988) 2444–2448.
[15] Y. Takakusagi, D. Manita, T. Kusayanagi, J. Izaguirre-Carbonell, K. Takakusagi, K. Kuramochi, K. Iwabata, Y. Kanai, K. Sakaguchi, F. Sugawara, Assay. Drug Dev. Technol. 11 (2013) 206–215.
[16] Y. Matsumoto, Y. Shindo, Y. Takakusagi, K. Takakusagi, S. Tsukuda, T. Kusayanagi, H. Sato, T. Kawabe, F. Sugawara, K. Sakaguchi, Bioorg. Med. Chem. 19 (23) (2011) 7049–7056.
[17] D. Manita, Y. Toba, Y. Takakusagi, Y. Matsumoto, T. Kusayanagi, K. Takakusagi, S. Tsukuda, K. Takada, Y. Kanai, S. Kamisuki, K. Sakaguchi, F. Sugawara, Bioorg. Med. Chem. 19 (24) (2011) 7690–7697.
[18] K. Morohashi, H. Sahara, K. Watashi, K. Iwabata, T. Sunoki, K. Kuramochi, K. Takakusagi, H. Miyashita, N. Sato, A. Tanabe, K. Shimotohno, S. Kobayashi, K. Sakaguchi, F. Sugawara, PLoS One 6 (4) (2011) e18285.
[19] K. Takakusagi, Y. Takakusagi, K. Ohta, S. Aoki, F. Sugawara, K. Sakaguchi, Protein Eng. Des. Sel. 23 (2) (2010) 51–60.
[20] Y. Takakusagi, K. Kuramochi, M. Takagi, T. Kusayanagi, D. Manita, H. Ozawa, K. Iwakiri, K. Takakusagi, Y. Miyano, A. Nakazaki, S. Kobayashi, F. Sugawara, K. Sakaguchi, Bioorg. Med. Chem. 16 (22) (2008) 9837–9846.
[21] T. Morimura, N. Noda, Y. Kato, T. Watanabe, T. Saitoh, T. Yamazaki, K. Takada, S. Aoki, K. Ohta, M. Ohshige, K. Sakaguchi, F. Sugawara, J. Antibiot. (Tokyo) 59 (10) (2006) 625–632.
[22] L. Verdier, J. Gharbi-Benarous, G. Bertho, N. Evrard-Todeschi, P. Mauvais, J.P. Girault, J. Chem. Soc. Perkin Trans. 2 (12) (2000) 2363–2371.
[23] Y. Kuroiwa, Y. Takakusagi, T. Kusayanagi, K. Kuramochi, T. Imai, T. Hirayama, I. Ito, M. Yoshida, K. Sakaguchi, F. Sugawara, PLoS One 8 (5) (2013) e63073.
[24] H. Chen, X. Su, K.G. Neoh, W.S. Choe, Anal. Chem. 78 (14) (2006) 4872–4879.
[25] K. Sano, K. Shiba, J. Am. Chem. Soc. 125 (47) (2003) 14234–14235.
[26] T. Kusayanagi, S. Tsukuda, S. Shimura, D. Manita, K. Iwakiri, S. Kamisuki, Y. Takakusagi, T. Takeuchi, K. Kuramochi, A. Nakazaki, K. Sakaguchi, S. Kobayashi, F. Sugawara, Bioorg. Med. Chem. 20 (21) (2012) 6248–6255.
[27] S. Moleirinho, W. Guerrant, J.L. Kissil, FEBS Lett. 588 (16) (2014) 2693–2703.
[28] W.G. Jiang, G. Watkins, A. Douglas-Jones, L. Holmgren, R.E. Mansel, BMC Cancer 6 (2006) 16.
[29] A. Bratt, O. Birot, I. Sinha, N. Veitonmaki, K. Aase, M. Ernkvist, L. Holmgren, J. Biol. Chem. 280 (41) (2005) 34859–34869.
[30] B. Troyanovsky, T. Levchenko, G. Mansson, O. Matvijenko, L. Holmgren, J. Cell Biol. 152 (6) (2001) 1247–1254.
[31] B.R. Zetter, J. Cell Biol. 152 (6) (2001) F35–F36.
[32] G.K. Aulakh, Y. Balachandran, L. Liu, B. Singh, Cell Tissue Res. 355 (2) (2014) 375–396.
[33] R. Benelli, M. Morini, F. Carrozzino, N. Ferrari, S. Minghelli, L. Santi, M. Cassatella, D.M. Noonan, A. Albini, FASEB J. 16 (2) (2002) 267–269.
[34] K. Nishiyama, Y. Takakusagi, T. Kusayanagi, Y. Matsumoto, S. Habu, K. Kuramochi, F. Sugawara, K. Sakaguchi, H. Takahashi, H. Natsugari, S. Kobayashi, Bioorg. Med. Chem. 17 (1) (2009) 195–202.
[35] S. Unezaki, R. Horai, K. Sudo, Y. Iwakura, S. Ito, Genes. Cells 12 (6) (2007) 773–785.
[36] R. Rivera-Pomar, H. Jackle, Trends Genet. 12 (11) (1996) 478–483.
[37] W.R. Ji, F.J. Castellino, Y. Chang, M.E. Deford, H. Gray, X. Villarreal, M.E. Kondri, D.N. Marti, M. Llinas, J. Schaller, R.A. Kramer, P.A. Trail, FASEB J. 12 (15) (1998) 1731–1738.
[38] Y. Cao, M.S. O'Reilly, B. Marshall, E. Flynn, R.W. Ji, J. Folkman, J. Clin. Invest. 101 (5) (1998) 1055–1063.
[39] M.S. O'Reilly, L. Holmgren, Y. Shing, C. Chen, R.A. Rosenthal, M. Moses, W.S. Lane, Y. Cao, E.H. Sage, J. Folkman, Cell 79 (2) (1994) 315–328.
[40] M. Arigoni, G. Barutello, S. Lanzardo, D. Longo, S. Aime, C. Curcio, M. Iezzi, Y. Zheng, I. Barkefors, L. Holmgren, F. Cavallo, Angiogenesis 15 (2) (2012) 305–316.
[41] T. Levchenko, N. Veitonmaki, A. Lundkvist, H. Gerhardt, Y. Ming, K. Berggren, A. Kvanta, R. Carlsson, L. Holmgren, FASEB J. 22 (3) (2008) 880–889.
[42] L. Holmgren, E. Ambrosino, O. Birot, C. Tullus, N. Veitonmaki, T. Levchenko, L.M. Carlson, P. Musiani, M. Iezzi, C. Curcio, G. Forni, F. Cavallo, R. Kiessling, Proc. Natl. Acad. Sci. U. S. A. 103 (24) (2006) 9208–9213.
[43] D.J. Rodi, R.W. Janes, H.J. Sanganee, R.A. Holton, B.A. Wallace, L. Makowski, J. Mol. Biol. 285 (1) (1999) 197–203.
[44] Y. Takakusagi, A. Suzuki, F. Sugawara, S. Kobayashi, K. Sakaguchi, World J. Eng. 5 (2009) 1005–1006.
[45] G. Stoesser, W. Baker, A. van den Broek, M. Garcia-Pastor, C. Kanz, T. Kulikova, R. Leinonen, Q. Lin, V. Lombard, R. Lopez, R. Mancuso, F. Nardone, P. Stoehr, M.A. Tuli, K. Tzouvara, R. Vaughan, Nucleic Acids Res. 31 (1) (2003) 17–22.

[46] S. Henikoff, J.G. Henikoff, Proc. Natl. Acad. Sci. U. S. A. 89 (22) (1992) 10915–10919.
[47] L. Makowski, Quantitative analysis of peptide libraries, in: V.A. Petrenko, G.P. Smith (Eds.), Phage Nanobiotechnology, RSC Publishing, Cambridge, United Kingdom, 2011, pp. 33–54.
[48] D.M. Carter, J.N. Gagnon, M. Damlaj, S. Mandava, L. Makowski, D.J. Rodi, P.D. Pawelek, J.W. Coulton, J. Mol. Biol. 357 (1) (2006) 236–251.
[49] D.J. Rodi, G.E. Agoston, R. Manon, R. Lapcevich, S.J. Green, L. Makowski, Comb. Chem. High. Throughput Screen. 4 (7) (2001) 553–572.